A Intelligent Nanorobots Fish Swarm Strategy for Tumor Targeting

ShanChao Wen[2], Yue Sun[1,2(✉)], SiYang Chen[1], and Yifan Chen[2,3]

[1] School of mechanical and electrical engineering, Chengdu University of Technology, Chengdu, China
sunyuestc90@126.com
[2] School of Life Science and Technology, University of Electronic Science and Technology of China, Chengdu, China
[3] Putian University, Putian, China

Abstract. This paper proposes a nanorobots fish swarm algorithm (NFSA) for tumor targeting. The alterations in the tumor microenvironment caused by tumor growth produce the biological gradient field (BGF), which is regulated by the adjacent tortuous and dense capillary network. NFSA is used to measure tumor-targeting efficiency in comparison to the benchmarks of Brute-force and the conventional gradient descent algorithm. Our goal is to increase the efficiency of targeting tumors in the early stages by using existing swarm intelligence algorithms to manipulate nanorobot swarms (NS) through magnetic fields. The extracorporeal observation system sensed the motion of NS under the influence of a BGF and then estimated the gradient of BGF. The invasive percolation algorithm models the vascular network to evaluate the performance of searching strategies. We also apply the exponential evolution step mechanism to boost the tumor-targeting efficiency of NFSA. The results show that NFSA has higher overall tumor targeting efficiency and a fast convergence property than previous algorithms. We hope that the NS in a multi-agent system could pave the way for challenges in tumor targeting.

Keywords: Tumor targeting · Nanorobots swarm · Biological gradient field · Vascular network · Swarm intelligence

1 Introduction

The high cancer mortality rate is primarily due to the diffusion and migration of malignant tumors [1]. Early therapy, for instance, can cut breast cancer mortality by 39%. As a result, early detection and diagnosis of malignancies can significantly improve the cancer cure rate. Since conventional medical imaging tools, such as Magnetic Resonance Imaging (MRI) and Computed Tomography (CT), are limited in accuracy and resolution, early tumor diagnosis is challenging. Consequently, magnetic nanoparticles (MNPs) play a critical role in medical imaging

Y. Chen et al. (Eds.): BICT 2023, LNICST 512, pp. 280–291, 2023.
https://doi.org/10.1007/978-3-031-43135-7_27

diagnostics today [2]. Under the guidance of a regulated magnetic field, MNPs as contrast agents may discriminate malignant tumors from healthy tissue.

Due to the high demand for oxygen and nutrients during malignant tumor growth, the capillaries growth surrounding the tumor is abnormal, forming and tortuous and high-density interconnected network. As a consequence, NS can penetrate the tumor region by passively permeating capillaries [3]. It is difficult to eradicate the NS since the tumor region lacks a regular lymphatic system. Accurate medical imaging and target drug delivery treatment can be accomplished once NS is enriched in the tumor's area.

Nanorobots in medical imaging provides a solution for early tumor detection and precise drug targeting. Based on tumor detection, Chen et al. [4] proposed an *in vivo* computing system, which achieves considerable aggregation of nanorobots in the tumor area with the shortest possible physiological path without previous knowledge of tumor location.

Because of the complicated human vascular network and biological milieu, an NS could easily be split into numerous smaller clusters of NS while propagation in the vascular network. Moreover, the tumor detection efficiency of a single NS is lower than that of multiple NS. As a result, a swarm intelligence-based multi-agent system for tumor targeting is required. A sequential evolutionary strategy is proposed in the [5], which is influenced by traditional wireless communication "time division multiplexing (TDM)" and creates a strict and realistic framework for tumor targeting in multi-NS management. Since the challenges of extracorporeal operating system in manipulating multiple NS separately, thus, this paper assumes all the NS under a uniform magnetic field control.

The biological population evolutionary algorithm is inspired by behaviors of the biological population in nature [6], which provides a solution for the swarm intelligent optimization. This paper proposes a multiple NS fish swarm strategy for tumor targeting, using sequential evolutionary methods and an artificial fish swarm algorithm.

The rest of this paper is organized as follows: The biological gradient field is illustrated in the Sect. 2. The vascular network modeling is established in the Sect. 3 using the invasive percolation algorithm. Moreover, the Sect. 4 describes the NFSA optimization approach in detail. The comparison of brute-force, conventional gradient algorithm, and NFSA are analyzed in the Sect. 5. We conclude in the Sect. 6 section with a proposal for future direction.

2 Biological Gradient Fields

2.1 The Generation of BGFs

Tumor lesions produce multi-property alterations to the tumor microenvironment, and the biological and chemical features of the near-site and far-site tumors are vastly different [7]. For example, in the tumor microenvironment, the distribution of oxygen density, pH, glucose, and other nutrients (such as growth factors and hormones) may be uneven or insufficient. These homologous tissue heterogeneities caused by malignancy can be thought of as BGF.

Through the tumor microenvironment's enhanced permeability and retention effect (EPR), NS with contrast agents can reach the area around the tumor via passive transport. Through the EPR effect of the tumor micro-environment, NS can be continuously enriched in tumor lesions [8].

2.2 BGF in Vivo Computing

NS does not directly sense the value of BGF, but it serves as a computational agent by measuring and estimating the changes in the features of NS [9]. For instance, the pH-responsive Oregon Green 488 (OG) conjugates with a trypsin-cleavable peptide as PH changes, acting as a biosensor to detect the dynamic of PH profile [10]. The extracorporeal operating system continually detect NS towards the tumor, depending on the BGF value. Since there are currently no commonly accepted quantitative models of BGF, this paper adopts the Sphere objective function with global minimization values to characterize BGF.

For the convenience of calculation, the BGF value is normalized to 0–1. The tumor search parameter space P is set to -5mm $\leq$ (x,y) $\leq$ 5 mm. The expression is as follows:
Landscape :

$$U_T(x,y) = \begin{cases} 1 & \sqrt{x^2+y^2} \leq 0.3 \ and \ (x,y) \in P \\ -(x^2+y^2+10)/85+1 & \sqrt{x^2+y^2} > 0.3 \ and \ (x,y) \in P \\ 0 & (x,y) \notin P \end{cases} \quad (1)$$

where space P denotes a discrete vascular network space. The Sphere function, smooth and uniform, is regarded as the most basic objective function. The circle with a radius of 0.3 mm in the central position is considered a tumor, and the objective function value of this region corresponds to the landscape's global maximum value 1, also the optimal global solution.

3 Vascular Network Around Tumor Micro-Environment

3.1 Growth Mechanism of Vascular Network Around Tumor Micro-Environment

Human tissues are supplied with oxygen and nutrients via the vascular network system. Capillaries, which connect arteries and veins, require more oxygen and nutrients than normal tissues due to tumor cells' erratic proliferation; hence their capillaries will suffer pathological structural changes. As a result, changes in the status of surrounding tissues can be reflected in the geometry of blood vessels. The otherwise normal vascular network may proliferate by budding or overlapping when the tumor diameter reaches 1–2 mm. The vascular networks near the tumor degrade significantly as the tumor grows. The blood vessels surrounding the tumor, on the other hand, will proliferate rapidly (Fig. 1).

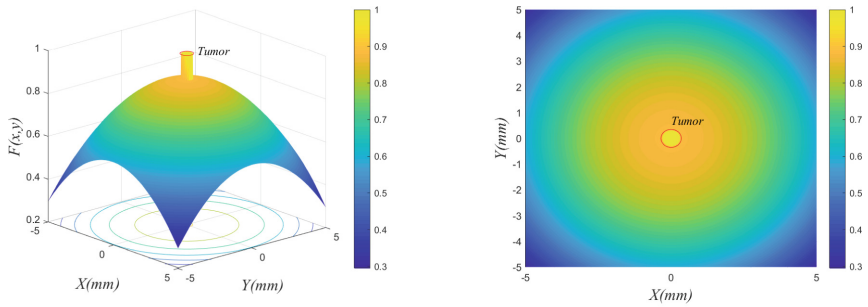

(a) (b)

Fig. 1. The diagram of the Sphere objective function: (a) the geometry of the Sphere function and (b) its contour curve

Pathological vascularity is one of the hallmarks of a potential tumor. The normal vascular network undergoes a series of tumor-specific changes in response to the demand for nutrients and oxygen for tumor growth, including vascular regeneration (formation of new blood vessels), vascular remodeling (integration of existing vessels with tumor vessels), and vascular degeneration. Furthermore, the permeability of these vascular networks is improved, and the diameter of their endothelial and extracellular pores is increased, allowing nanoparticles to pass through the pore and reach the tumor lesion. In summary, malignant tumor vasculature is characterized by the following two features:

- **1) The density of blood vessels in the paratumoral area is greater than in normal tissue.**
- **2) The centeral area of tumor suffered vascular degeneration.**

3.2 Modeling of Vascular Network Periphery of the Tumor

We assume that the capillary network around normal tissues is latticed and regularized, and the vascular network's growth direction is parallel to the coordinate axis. The distance between capillaries determines the capillaries density. The expected increase in capillaries density is usually observed in the periphery area of the tumor, whereas the morphology of the vasculature in the tumor center is characterized by decreased density [11]. The intrusive percolation algorithm presents the characteristics of blood vessels with tumors, which is used to construct the near-tumor capillary network [12].

In the intrusion percolation model, each lattice point is randomly assigned a uniformly distributed intensity value. Then from the set position as the starting point, the vessel grows to the position with the smallest lattice intensity among all the lattice nodes adjacent to the current network. The procedure is repeated until the desired level of lattice occupancy is achieved. The lattice occupation is used to simulate the fractal dimension of the pathological vascular network of the tumor. The fractal dimensions 1.6, 1.8, and 1.9 correspond to 40%, 60%, and

80%of the lattice occupation, respectively. To create a realistic blood vascular network, the size of the pathological vascular network set in this paper is the space P_m of –1 mm ≤ (x,y) ≤ 1 mm, while P_{m1} represents the para-tumor blood vessels. P_{m2} is expressed as the blood vessel in the central area surrounding the tumor.$P_{m1}, P_{m2} \in P_m$. The lower-left corner of the blood vessel is the NS injection area, the range of which is –5 mm ≤ (x,y) ≤ –4 mm, as shown in Fig. 2,

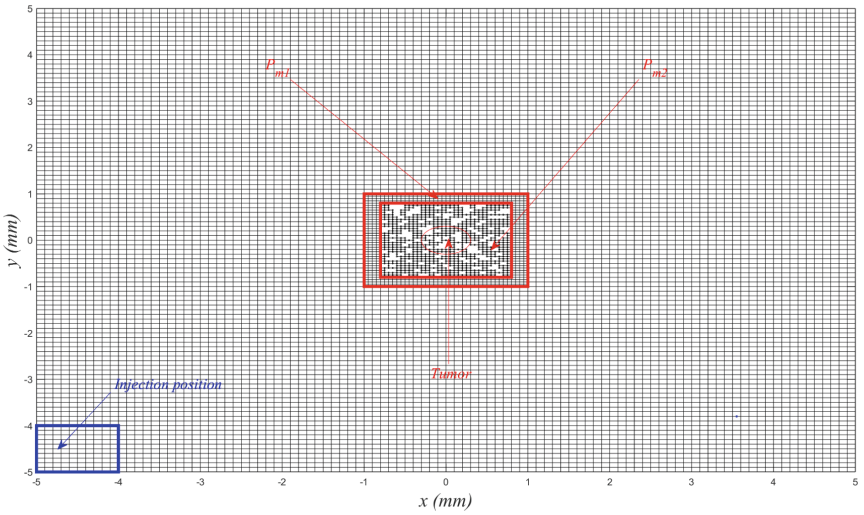

Fig. 2. The vascular network is modeled by invasive percolation technique. P_{m1} represents the blood vessels adjacent to the tumor, P_{m2} represents the blood vessels in the central area of the tumor, and the lower left corner of the blood vessel is the NS injection area.

4 Computing Method of Nano Fish Swarm Algorithm

Although the uniform magnetic field generated by the Helmholtz coil can regulate the movement direction of NS, the best orientations of multiple NS are frequently incongruent. As a result, while the magnetic field may cause one NS to move in the optimal direction, the magnetic field will cause other NS to move in the non-optimal direction. Based on this, this paper adopts the control method of time-division multiplexing proposed in [5]. The critical parts of the model are divided into the following points.

4.1 Time Division Multiplexing Control Strategy

The whole framework of the time-division multipurpose control model is divided into three modes: FC (Forced Control), DC (Directional Control), and IT (ImagingTracking). In IT mode, Multiple NS move through blood viscous force without

the intervention of a magnetic field, and BGF can be calculated by an extracorporeal operating system based on NS's performance; In DC mode, The magnetic field controls the NS in a specific order. However, in a cycle, the magnetic field only cares about whether the movement direction of one NS is optimal and ignores the other NS. In FC mode, the motion of NS is similar to that in DC mode. A cluster of NS moves in the same direction as the one NS under the uniform magnetic field control, which may result in a non-optimal direction. The rest of NS, in this case, is also called in forced control.

- 1) **Initialization**: at the initial time $t_{DC,1}^{(1)}$, nano-particle swarm NS_1,NS_2,..., NS_N enters the injection area, randomly allocates each position in the injection area, and uses the vector $\overrightarrow{x_1}(t_{DC,1}^{(1)})$, $\overrightarrow{x_2}(t_{DC,1}^{(1)})$, $\overrightarrow{x_3}(t_{DC,1}^{(1)})$,..., $\overrightarrow{x_N}(t_{DC,1}^{(1)})$ represent its initial position, where the superscript indicates the number of times of current evolution for all NS; when all NS completes a FC\DC-IT movement, it is regarded as evolutionary completion and enters the next generation; subscript is the number of times of cycles in current generation.
- 2) **Directional control (DC)**: NS_1 is used as a representative to depict the motion process since all NS are controlled in the same way. The initial position of NS_1 is $\overrightarrow{x_1}(t_{DC,1}^{(1)})$, and after a DC control, the position changes $\overrightarrow{x_1}(t_{DC,1}^{(1)}) \rightarrow \overrightarrow{x_1}(t_{IT,1}^{(1)})$, where $t_{IT,1}^{(1)} = t_{DC,1}^{(1)} + T_{FC/DC,1}^{(1)}$, $T_{FC/DC,1}^{(1)}$is the control time, the control time is not necessarily fixed, and this parameter can be adjusted to meet the needs of the situation. Under the vascular network shown in Fig. 2, the specific location of the NS_1 is calculated as follows:

$$\overrightarrow{x_1}(t_{IT,1}^{(1)}) = \overrightarrow{x_1}(t_{DC,1}^{(1)}) + d_1(t_{DC,1}^{(1)})\overrightarrow{u}_{\angle\varphi(t_{DC,1}^{(1)})} + \overrightarrow{e_1}(t_{DC,1}^{(1)}) \tag{2}$$

$$\left\| d_1(t_{DC,1}^{(1)}) \right\|_1 = v_{ma} \cdot T_{DC/FC,1}^{(1)} \tag{3}$$

$$\left\| d_1(t_{DC,1}^{(1)}) \right\|_1 = d_1(t_{DC,1}^{(1)}) \cos\angle\varphi(t_{DC,1}^{(1)}) + d_1(t_{DC,1}^{(1)}) \sin\angle\varphi(t_{DC,1}^{(1)}) \tag{4}$$

where $\|\bullet\|_1$ indicates l_1 norm, $\angle\varphi(t_{DC,1}^{(1)})$ depends on the optimization direction needed by the situation, $\overrightarrow{u}_{\angle\varphi(t_{DC,1}^{(1)})}$ is the unit vector in the optimization direction, between 0 and $\pi/2$, since NS could not perform the opposite direction of blood flow. The discretization error generated by the discretization of the vascular network, to ensure that the destination is on the vascular node, is $e_1(t_{DC,1}^{(1)})$, and the magnetic field control speed is v_{ma}.
- 3) **Imaging tracking (IT)**: when a FC\DC movement occurs, the extracorporeal control system needs to re-track all the NS to calculate the motion direction of the next optimization. At this stage, the NS walk randomly along the blood flow velocity to sense the BGF. After the completion of the IT, the position change of the NS_1 is $\overrightarrow{x_1}(t_{IT,1}^{(1)}) \rightarrow \overrightarrow{x_1}(t_{DC,2}^{(1)})$, where $t_{DC,2}^{(1)} = t_{IT,1}^{(1)} + T_{IT,1}^{(1)}$ traveling $T_{IT,1}^{(1)}$ is the walking time, which is similar to that of $T_{FC/DC,1}^{(1)}$. The specific calculation method is as follows:

$$\overrightarrow{x_1}(t_{DC,2}^{(1)}) = \overrightarrow{x_1}(t_{IT,1}^{(1)}) + (x(t_{IT,1}^{(1)}), y(t_{IT,1}^{(1)})) \tag{5}$$

$$\left\| d_1(t_{IT,1}^{(1)}) \right\|_1 = v_{vessel} \cdot T_{IT,1}^{(1)} + e(t_{IT,1}^{(1)}) \tag{6}$$

$$\left\| d_1(t_{IT,1}^{(1)}) \right\|_1 = x(t_{IT,1}^{(1)}) + y(t_{IT,1}^{(1)}) \tag{7}$$

where v_{vessel} is the blood flow velocity of the vascular network, and the blood flow velocity of blood vessels in different regions is different, and the error compensation of $e(t_{IT,1}^{(1)})$ node is to ensure that the movement destination is on the vessel node. $\left\| d_1(t_{IT,1}^{(1)}) \right\|_1$ is the distance of NS flowing with blood in it mode. Since NS moves up or right in the vascular network under the influence of blood viscous force. The value of $x(t_{IT,1}^{(1)}), y(t_{IT,1}^{(1)})$ is equally distributed under the constraint of (7).

– 4) **Forced control (FC)**: this mode can be regarded as the DC control stage of other NS, at this time, due to the global force of the magnetic field, the NS_1 will be forced to move. After the completion of the FC, the position of the NS1 changes to $\overrightarrow{x_1}(t_{DC,2}^{(1)}) \rightarrow \overrightarrow{x_1}(t_{IT,2}^{(1)})$, $t_{IT,2}^{(1)} = t_{DC,2}^{(1)} + T_{FC/DC,2}^{(1)}$, $T_{FC/DC,2}^{(1)}$ is the control time of other NS, and the specific position calculation rule of NS is similar to that of the DC mode.

4.2 Nanorobot Fish Swarm Algorithm

NFSA is an algorithm that combines an artificial fish swarming algorithm with a time-division multiplexing control strategy. The artificial fish swarm algorithm is proposed based on the swarm behavior of fish, where the clustering and foraging behavior in artificial fish swarm algorithm (AFSA) can be combined with the swarm intelligence control of NS [13]. In order to ensure the targeting efficiency of the whole population, NFSA adopts a piecewise iterative method in the DC phase based on the time-division multiplexing strategy and the specific process is shown in Fig. 3 In DC mode, there are two control types: foraging (DC_c) and clustering (DC_b). In foraging behavior, the sequential control strategy is adopted, and NS_1, NS_2... NS_N adjusts its orientation sequentially. Under foraging behavior, The direction with the fastest fitness increase is given precedence by NS. The weakest-first evolutionary strategy is adopted under clustering behavior. Individuals with the worst BGF adaptation are given priority in moving to the center of m NS with the best adaption. This design is because some NS with the best BGF fitness tend to enter the tumor center first, which has more convoluted blood capillaries. The movement of these NS is more likely to be restricted by vascular space, which is favorable for allowing NS with low BGF fitness to catch up and approach tumor lesions as much as possible, enhancing the targeting rate of all NS. The duration T_{DC_c} of foraging behavior tends to influence the improvement of the best NS fitness, while the duration T_{DC_b} of clustering behavior tends to influence the improvement of the fitness of all NS. How to balance T_{DC_c} and T_{DC_b} duration to maximize the targeting efficiency

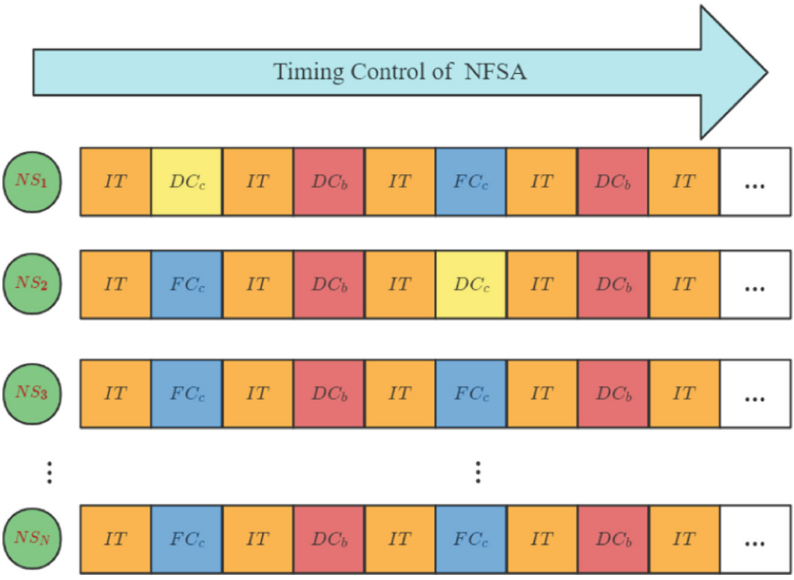

Fig. 3. Timing control logic of NFSA

needs deeper level related research. Taking NS1 as an example, the specific calculation model of clustering behavior (DC_b) and foraging behavior (DC_c) is as follows:

Foraging behavior

$$\overrightarrow{u}_{\angle\varphi(t_{DC,1}^{(1)})} = \frac{grad(f(\overrightarrow{x_1}(t_{DC,1}^{(1)})))}{\left|grad(f(\overrightarrow{x_1}(t_{DC,1}^{(1)})))\right|} \tag{8}$$

Clustering behavior

$$\overrightarrow{u}_{\angle\varphi(t_{DC,1}^{(1)})} = \frac{\frac{\sum_{j\in V_m}\overrightarrow{x_j}(t_{DC,1}^{(1)})}{m} - \overrightarrow{x_1}(t_{DC,1}^{(1)}))}{\left|\frac{\sum_{j\in V_m}\overrightarrow{x_j}(t_{DC,1}^{(1)})}{m} - \overrightarrow{x_1}(t_{DC,1}^{(1)}))\right|} \tag{9}$$

where V_m is the set of m NS with the best fitness. Until they reach the tumor, all ns are subjected to continual iterative control in the manner indicated in Fig. 3.

5 Comparison and Performance Analysis of Algorithms

5.1 Simulation Parameter Setting

Numerical simulations are performed in MatLab to compare the performance of NFSA, conventional GD algorithm, and Brute-force search for tumor targeting.

The network vessels used are shown in Fig. 2. The direction of blood flow is from lower left to upper right. The distance between capillaries far away from the tumor is 0.1mm, and the minimum distance between capillaries near the tumor is 0.05mm. Detailed simulation parameters are given in Table 1. In the evaluation

Table 1. Parameter Settings

Parameters	Numerical values
Duration of the IT phase	4 s
maximum number of iterations	15
The number of NS	5
The velocity near the tumor V_{Pm}	50 μm/s
The velocity away from the tumor V	200 μm/s
The number of optimal NS selected m	2

of tumor-targeting efficiency, the parameters P_d and η are considered within a limited number of iterations, whereas P_d represents the ratio of the number of successful tumor detection to the total number of simulation experiments, and η denotes the ratio of the total number of computational agents that detected the tumor to the total number of NS. The random direction of range $0 - \frac{\pi}{2}$ is employed in the DC phase, taking into account the influence of Brute-force search as a reference group and blood flow velocity. In addition, since the tumor diameter is too small, the change step of the exponential evolution mechanism is also adopted in the DC/FC stage.

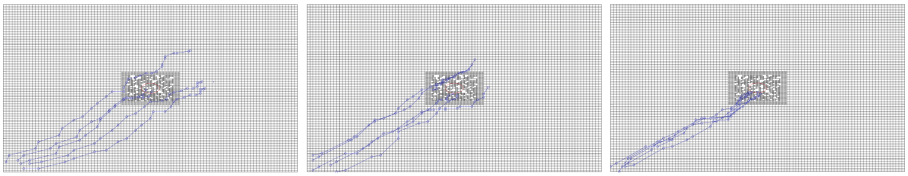

(a) (b) (c)

Fig. 4. Multiple NS paths with three strategies in one simulation: (a) Multiple NS paths using Brute-force search; (b) Multiple NS paths using traditional GD algorithm in TDM Framework; (c) Multiple NS paths using AFSA

5.2 Simulation Results

Figure 4 shows the NS path trajectory performed in one simulation using the three algorithms. Figure 5 shows the corresponding average fitness, the average

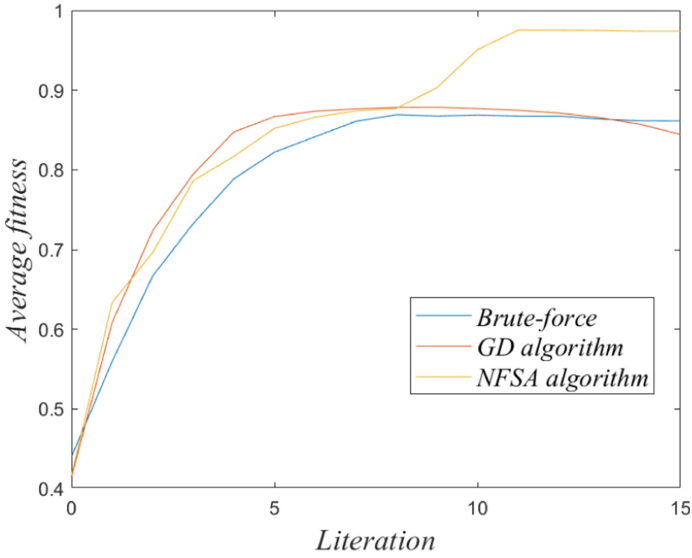

Fig. 5. The change of the average fitness of multiple NS as the number of iterations increases under different strategies

value of BGF, with increasing number of iterations. Figure 6 presents the histogram of the distribution of the number of NS that can reach the central region of the tumor using the three algorithms in 100 experiments, and the path of Brute-force search is scattered since the direction of magnetic field control in its DC phase is random. The overall targeting efficiency of the NFSA-based swarm intelligence system is significantly higher than that of the GD method and Brute-force search, as shown in Fig. 6. The NS in the DC phase uses the GD algorithm to move in the same direction as its gradient, whereas the other NS in the FC phase is offset due to the global action of the magnetic field force. As a result, the total targeting efficiency of multi-NS systems using the time-division multiplexing technique and the GD algorithm is average. In the multiple NS system based on the NFSA algorithm, when the optimal NS is close to the tumor area or the tumor center area. The movement of optimal NS is restricted to capillary degradation around the tumor. Simultaneously, the NS with the lowest fitness is chosen to approach some of the best NS. Even though the global magnetic field impacts it, the most optimal NS status is unaffected, and the overall NS targeting rate can be improved.

From Fig. 5, Although the average fitness of NS employing Brute-force search improves over time as a result of blood flow, its targeting rate remains low. The fitness will rapidly decline once they pass through the tumor. In contrast, the convergence speed of multiple NS systems using the time-division multiplexing strategy and GD algorithm is the fastest since BGF usually changes fastest in the gradient direction. However, unable to overcome the effect of the global force of the magnetic field, the average fitness decreases rapidly after passing through

the tumor, as shown in Fig. 5. After some iterations in NFSA, the advantages of the piecewise iteration strategy start to emerge. The foraging behavior (DC_c) ensures a better convergence rate of the multi-NS system, while the clustering behavior (DC_b) ensures the overall tumor targeting efficiency of the system.

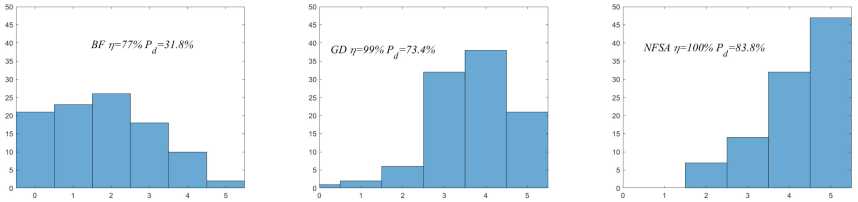

Fig. 6. Multi-NS paths with three strategies under one simulation: (a) Targeting efficiency using Brute-force search of 100 experiments; (b) Targeting efficiency using traditional GD algorithm of 100 experiments; (c) Targeting efficiency using AFSA of 100 experiments

6 Conclusion

In this paper, NFSA is proposed in the framework of TDM strategy and artificial fish swarm algorithm, which provides an effective multi-agent system for tumor targeting. The vascular network periphery of the tumor is tortuous and dense interconnected, which is a considerable challenge to controlling the NS swarm. The simulation results demonstrate that the swarm intelligence system based on NFSA has considerable search convergence speed and more optimized overall tumor targeting efficiency than the traditional GD algorithm and Brute-force search. We may apply more evolutionary algorithms and more complex fractal blood vessels to provide more practical and effective tumor targeting programs in future work.

References

1. Smith, R., et al.: Cancer screening in the United States, 2019: a review of current American cancer society guidelines and current issues in cancer screening. CA Cancer J. Clin. **69**, 184–210 (2019)
2. Sun, Y., Qing, Y., Chen, Y.: In vivo computing for smart tumor targeting in taxicab-geometry vasculature. IEEE Trans. NanoBiosci. **21**, 445–453 (2022)
3. Harney, A.S., et al.: Real-time imaging reveals local, transient vascular permeability, and tumor cell intravasation stimulated by tie2hi macrophage-derived VEGFA. Cancer Disc. **5**(9), 932–943 (2015). ISSN 2159–8274
4. Chen, Y., et al.: Biosensing-by-learning direct targeting strategy for enhanced tumor sensitization. IEEE Trans. NanoBiosci. **18**(3), 498–509 (2019)

5. Shi, S., et al.: Exponential evolution mechanism for in vivo computation. Swarm Evol. Comput. **65**, 100931 (2021). ISSN 2210–6502
6. Simon, D.: Evolutionary optimization algorithms: biologically-inspired and population-based approaches to computer intelligence (2013)
7. Ali, M., Chen, Y., Cree, M.J.: Autonomous *In Vivo* computation in internet of nano bio things. IEEE Internet Things J. **9**(8), 6134–6147 (2022)
8. Ao, H., et al.: Enhanced tumor accumulation and therapeutic efficacy of liposomal drugs through over-threshold dosing. J. Nanobiotechnol. **20**, 137 (2022). https://doi.org/10.1186/s12951-022-01349-1
9. Bejarano, L., Jordão, M.J.C., Joyce, J.A.: Therapeutic targeting of the tumor microenvironment. Cancer Disc. **11**(4), 933–959 (2021). ISSN 2159–8274
10. Sun, Y., Bian, H., Chen, Y.: A photolysis-assist molecular communication for tumor biosensing. Sensors **22**(7), 2495 (2022)
11. Paul, R.: Flow-correlated dilution of a regular network leads to a percolating network during tumor-induced angiogenesis. Eur. Phys. J. E Soft Matter **30**(1), 101–114 (2009). https://doi.org/10.1140/epje/i2009-10513-8. ISSN 1292–8941
12. Shi, S., et al.: Nanorobots-assisted tumor sensitization and targeting for multifocal tumor, pp. 362–365 (2020)
13. Liu, Y., et al.: Parameter identification of collaborative robot based on improved artificial fish swarm algorithm. In: 2020 International Conference on High Performance Big Data and Intelligent Systems (HPBD IS), pp. 1–7 (2020)